Spin relaxation in gases due to inhomogeneous static and oscillating magnetic fields

G. D. Cates, D. J. White, Ting-Ray Chien, S. R. Schaefer, and W. Happer
Department of Physics, Princeton University, Princeton, New Jersey 08544
(Received 27 June 1988)

We have extended a recent theory of spin relaxation in gases due to static magnetic field inhomogeneities to include the effects of oscillating magnetic fields. We use this theory to show how magnetic field inhomogeneities cause spin relaxation under magnetic resonance conditions. We have confirmed some of the main theoretical predictions by experimental observations. Spin relaxation in inhomogeneous magnetic fields can be used as a convenient new way to measure diffusion constants in gases.

I. INTRODUCTION

In a recent paper, Cates *et al.*[1] derived expressions for the relaxation rates of polarized spins due to static magnetic field inhomogeneities in gases at low and high pressures. This work was a generalization of earlier work by Gamblin and Carver[2] and by Schearer and Walters,[3] who developed the theory of longitudinal spin relaxation due to static inhomogeneities at high gas pressures. Questions relating to spin relaxation due to magnetic field inhomogeneities have also been considered by Barbé, Leduc, and Laloë[4,5] and by Lefèvre-Seguin, Nacher, and Laloë.[6] In practice, spins are frequently subject to oscillating magnetic fields, for example, ambient 60-Hz fields, or oscillating magnetic resonance fields. Even if the oscillating field is perfectly homogeneous, the longitudinal relaxation rate can be greatly accelerated under magnetic resonance conditions, since the static field inhomogeneities are transformed into static and oscillating field inhomogeneities in the small, effectively static "holding field" of the rotating coordinate system. In this paper we extend the analysis of Cates *et al.*,[1] which we shall refer to as CSH, to include the effects of oscillating magnetic fields. We use these new results to discuss how magnetic field inhomogeneities cause spin relaxation during magnetic resonance conditions. In Sec. III we discuss experiments which have been designed to test the main predictions of the theory. There is very good agreement between theory and experiment. The results of this paper show that the quantitative study of spin relaxation in known magnetic field inhomogeneities is a precise and convenient way to measure the diffusion constants of noble gases in various gaseous mixtures. The technique we suggest differs from earlier work[5] in that we explicitly derive limits in which the spin relaxation is independent of the cell radius. In certain experimental conditions, the dependence on the cell radius R can be as great as R^4, making the cell radius a dominating source of systematic error.

II. THEORY

Since the analysis of spin relaxation in the presence of oscillating magnetic fields is an extension of the work of CSH, we shall only outline the steps which differ substantially from CSH, and we will refer to the results of that paper for background details. We assume that the total magnetic field $\mathbf{B}(\mathbf{r},t)$ at a position r within the cell and at a time t is the sum of a static mean field $\mathbf{B}_0$ and a static inhomogeneous field $\mathbf{B}_1(\mathbf{r})$, both of which were discussed in CSH, and an oscillating magnetic field which is the sum of two real, vector fields, an in-phase field $\mathbf{B}_2'$, and a quadrature field $\mathbf{B}_2''$, both oscillating at the frequency ω. We can write the oscillating part of the field as

$$\mathbf{B}(\mathbf{r},t)-\mathbf{B}_0-\mathbf{B}_1(\mathbf{r})=\mathbf{B}_2'(\mathbf{r})\cos\omega t+\mathbf{B}_2''(\mathbf{r})\sin\omega t$$
$$=\mathbf{B}_2(\mathbf{r})e^{-i\omega t}+\mathbf{B}_2^*(\mathbf{r})e^{i\omega t}\ . \tag{1}$$

The complex vector field amplitudes are

$$\mathbf{B}_2(\mathbf{r})=\tfrac{1}{2}[\mathbf{B}_2'(\mathbf{r})+i\mathbf{B}_2''(\mathbf{r})] \tag{2}$$

and

$$\mathbf{B}_2^*(\mathbf{r})=\tfrac{1}{2}[\mathbf{B}_2'(\mathbf{r})-i\mathbf{B}_2''(\mathbf{r})]\ . \tag{3}$$

The complex field amplitude will be associated with a complex Larmor frequency

$$\mathbf{\Omega}_2(\mathbf{r})=\frac{g_K\mu_B}{\hbar}\mathbf{B}_2(\mathbf{r})=\lambda\mathbf{B}_2(\mathbf{r})\ , \tag{4}$$

where $\lambda=g_K\mu_B/\hbar$ is the gyromagnetic ratio of the spins. Then the spin Hamiltonian of the atoms is

$$H=H^{(0)}+H^{(1)}+Ve^{-i\omega t}+V^\dagger e^{i\omega t}=\hbar\mathbf{\Omega}\cdot\mathbf{L}\ , \tag{5}$$

where the unperturbed Hamiltonian $H^{(0)}$ describes the rotation of the spins about the z axis at the mean Larmor frequency Ω_0,

$$H^{(0)}=\hbar\Omega_0 L_z\ . \tag{6}$$

The perturbation due to static field inhomogeneities is

$$H^{(1)}=\hbar\mathbf{\Omega}_1\cdot\mathbf{L}\ . \tag{7}$$

The perturbation amplitude of the oscillating field is

$$V=\hbar\mathbf{\Omega}_2\cdot\mathbf{L}\ . \tag{8}$$

In summary, the Larmor frequency $\mathbf{\Omega}$ of (5) is

$$\mathbf{\Omega}=\Omega_0\hat{\mathbf{z}}+\mathbf{\Omega}_1+\mathbf{\Omega}_2e^{-i\omega t}+\mathbf{\Omega}_2^*e^{+i\omega t}\ . \tag{9}$$

As in Eq. (16) of CSH we assume that the spin polarization evolves because the spins rotate at the frequency Ω while they diffuse through the gas. The rate of change of the spin-density matrix is given by Eq. (16) of CSH, which we rewrite as

$$\frac{\partial}{\partial t}|\rho)=(-i\Omega\cdot\mathbf{L}+D\nabla^2)|\rho) , \tag{10}$$

where D is the diffusion coefficient of the spins in the gas. To simplify the subsequent analysis of relaxation in the rotating coordinate system, we have written the density matrix as a vector $|\rho)$ in polarization space instead of an operator ρ in spin space. This amounts to making the replacement $[K_i,\rho]\rightarrow L_i|\rho)$ where K_i is a spin angular momentum operator and L_i is the corresponding angular momentum operator for polarization space.

We see an exponentially decaying solution to (10) of the form

$$|\rho)=\sum_{j,q}|j)f_{jq}(\mathbf{r})e^{-(\gamma-i\omega q)t} , \tag{11}$$

where $|j)=|LM)$, an irreducible spherical tensor,[7] is one of the eigenpolarizations defined by Eq. (19) of CSH. Equation (11) differs from the analogous equation (23) of CHS since it contains terms oscillating at the integer multiples q of the perturbation frequency ω. These terms represent the spins in the process of exchanging q photons with the oscillating field. In analogy to Eqs. (26) and (27) of CSH we expand the damping rate γ and the mode amplitudes f_{jq} as power series in the perturbation amplitudes Ω_1 and Ω_2. The mode amplitudes of various orders are determined by equations analogous to Eqs. (28)–(30) of CSH. The zeroth-order mode amplitudes satisfy the partial differential equation

$$(D\nabla^2-i\Lambda_i-i\omega p+\gamma^{(0)})f_{ip}^{(0)}=0 . \tag{12}$$

The first-order mode amplitudes are determined by

$$(D\nabla^2-i\Lambda_i-i\omega p+\gamma^{(0)})f_{ip}^{(1)}+\gamma^{(1)}f_{ip}^{(0)}+\frac{1}{i\hbar}\sum_j H_{ij}^{(1)}f_{jp}^{(0)}+\frac{1}{i\hbar}\sum_j V_{ij}f_{j,p+1}^{(0)}+\frac{1}{i\hbar}\sum_j V_{ij}^{\dagger}f_{j,p-1}^{(0)}=0 . \tag{13}$$

The second-order mode amplitudes are determined by

$$(D\nabla^2-i\Lambda_i-i\omega p+\gamma^{(0)})f_{ip}^{(2)}+\gamma^{(1)}f_{ip}^{(1)}+\gamma^{(2)}f_{ip}^{(0)}+\frac{1}{i\hbar}\sum_j H_{ij}^{(1)}f_{jp}^{(1)}+\frac{1}{i\hbar}\sum_j V_{ij}f_{j,p+1}^{(1)}+\frac{1}{i\hbar}\sum_j V_{ij}^{\dagger}f_{j,p-1}^{(1)}=0 . \tag{14}$$

The mode amplitudes satisfy the boundary condition (25) of CSH, which we rewrite as

$$\frac{\partial f_{ip}^{(n)}}{\partial n}=0 . \tag{15}$$

The normal derivative vanishes at the cell walls, because we assume that the cell walls cause negligible spin relaxation.

For concreteness we will assume, as in CSH, that the sample cell is spherical. Other simple cell shapes can be analyzed in a similar way, and a detailed discussion of cylindrical cells was given in a related paper by Wu *et al.*[8] There will be a zeroth-order solution to (12) of the form

$$f_{jq;\alpha ip}^{(0)}=\phi_\alpha\delta_{ji}\delta_{qp} , \tag{16}$$

for every combination of a diffusion index α, which represents the spatial quantum numbers $l\mu n$ of a diffusion mode [Eq. (37) of CSH] of a spherical cell, a polarization index i which represents the multipole quantum numbers LM of the irreducible basis tensors [Eq. (19) of CSH], and a photon index p, which represents the number of photons of the oscillatory field which are being exchanged with the spins. The corresponding decay rates are given by Eq. (32) of CSH as

$$\gamma_{\alpha ip}^{(0)}=Dk_\alpha^2+i\Lambda_i+i\omega p=\frac{Dx_{1n}^2}{R^2}+i\Omega_0 M+i\omega p , \tag{17}$$

where x_{1n} is the nth solution to $dj_1(x)/dx=0$. We may write the nth-order corrections to the polarization amplitudes as superpositions of the zeroth-order diffusion modes ϕ_β of a sphere, which were defined by Eq. (37) of CSH,

$$f_{jq;\alpha ip}^{(n)}=\sum_\beta \phi_\beta a_{\beta jq;\alpha ip}^{(n)} . \tag{18}$$

Substituting (18) into (13), we find in analogy to Eq. (43) of CSH

$$(\gamma_{\alpha ip}^{(0)}-\gamma_{\beta jq}^{(0)})a_{\beta jq;\alpha ip}^{(1)}+\gamma_{\alpha ip}^{(1)}\delta_{\alpha\beta}\delta_{ij}\delta_{pq}+\frac{1}{i\hbar}\langle\beta|H_{ji}^{(1)}|\alpha\rangle\delta_{qp}+\frac{1}{i\hbar}\langle\beta|V_{ji}|\alpha\rangle\delta_{q,p-1}+\frac{1}{i\hbar}\langle\beta|V_{ji}^{\dagger}|\alpha\rangle\delta_{q,p+1}=0 , \tag{19}$$

where the matrix element of the oscillating perturbation is defined in analogy to Eq. (22) of CSH as

$$\langle\beta|V_{ji}|\alpha\rangle=\int d^3r\,\phi_\beta^* V_{ji}\phi_\alpha . \tag{20}$$

The integral extends over all volume elements d^3r of the sample cell.

As in the case of purely static field inhomogeneities, the first-order correction $\gamma_{0ip}^{(1)}$ to the damping rate of the uniform mode is zero. In analogy to Eq. (50) of CSH we find that the second-order correction is

$$\gamma_{0ip}^{(2)}=\sum_{\beta,j}{}'\frac{\langle 0|H_{ij}^{(1)}|\beta\rangle\langle\beta|H_{ji}^{(1)}|0\rangle}{\hbar^2(\gamma_{\beta jp}^{(0)}-\gamma_{0ip}^{(0)})}+\sum_{\beta,j}{}'\frac{\langle 0|V_{ij}^{\dagger}|\beta\rangle\langle\beta|V_{ji}|0\rangle}{\hbar^2(\gamma_{\beta j,p-1}^{(0)}-\gamma_{0ip}^{(0)})}+\sum_{\beta,j}{}'\frac{\langle 0|V_{ij}|\beta\rangle\langle\beta|V_{ji}^{\dagger}|0\rangle}{\hbar^2(\gamma_{\beta j,p+1}^{(0)}-\gamma_{0ip}^{(0)})} , \tag{21}$$

where the prime means that terms with vanishing denominators are to be excluded from the sum.

We will assume that the oscillating field is nearly homogeneous so that we can write in analogy to Eq. (51) of CSH

$$\mathbf{\Omega}_2(\mathbf{r})=\mathbf{\Omega}_2(0)+\mathbf{r}\cdot\nabla\mathbf{\Omega}_2(0)\ . \tag{22}$$

In contrast to the case considered in CSH of a static field inhomogeneity, which has $\mathbf{\Omega}_1(0)=0$, there can be a nonzero mean value $\mathbf{\Omega}_2(0)\neq 0$ of the oscillating magnetic field. The nonzero matrix elements of (8) therefore include, in addition to a term analogous to Eq. (54) of CSH, a term which involves no change of the diffusional quantum number

$$\langle 1\mu n\mid V_{LM',LM}\mid 0\rangle=\sqrt{L(L+1)}C(L1L;M,M'-M)\left[\delta_{l1}N_{1n}\frac{j_1(x_{1n})}{x_{1n}^2}\hbar R\,[\mathbf{x}_\mu\cdot\nabla(\Omega_2^*)_{M'-M}]^*+\delta_{l0}\delta_{\mu 0}[(\Omega_2^*)_{M'-M}]^*\right], \tag{23}$$

where C denotes a Clebsch-Gordan coefficient.[9] We also note the relation

$$[(\Omega_2)_\mu]^*=(-1)^\mu(\Omega_2^*)_{-\mu}\ , \tag{24}$$

between the spherical components of the complex vector $\mathbf{\Omega}_2$ and its complex-conjugate vector $\mathbf{\Omega}_2^*$.

The first term of (21) was evaluated in Eqs. (55) and (56) of CSH. If we evaluate the last two terms of (21) in an analogous way, we find that the total relaxation rate, due to the static field inhomogeneity $\mathbf{\Omega}_1$ and the oscillating field $\mathbf{\Omega}_2$, is

$$\begin{aligned}\mathcal{R}\gamma_{0,LM}^{(2)}=&\frac{8M^2R^4\mid\nabla\Omega_{1z}\mid^2}{175D}+\sum_n\frac{D[L(L+1)-M^2]}{(x_{1n}^2-2)}\left[\frac{\mid\nabla\Omega_{1x}\mid^2+\mid\nabla\Omega_{1y}\mid^2}{D^2x_{1n}^4R^{-4}+\Omega_0^2}\right]\\&+\sum_n\frac{D[L(L+1)-M^2]}{(x_{1n}^2-2)}\left[\frac{\mid\nabla\Omega_{2-}\mid^2}{D^2x_{1n}^4R^{-4}+(\Omega_0-\omega)^2}\right]+\sum_n\frac{4DM^2}{(x_{1n}^2-2)}\left[\frac{\mid\nabla\Omega_{2z}\mid^2}{D^2x_{1n}^4R^{-4}+\omega^2}\right]\\&+\sum_n\frac{D[L(L+1)-M^2]}{(x_{1n}^2-2)}\left[\frac{\mid\nabla\Omega_{2+}\mid^2}{D^2x_{1n}^4R^{-4}+(\Omega_0+\omega)^2}\right].\end{aligned} \tag{25}$$

The imaginary part of the damping (a frequency shift) is

$$\begin{aligned}\mathcal{I}\gamma_{0,LM}^{(2)}=&M\delta\Omega_0\\=&MR^2\Omega_0\sum_n\frac{\mid\nabla\Omega_{1x}\mid^2+\mid\nabla\Omega_{1y}\mid^2}{x_{1n}^2(x_{1n}^2-2)(D^2x_{1n}^4R^{-4}+\Omega_0^2)}\\&+\sum_n\frac{MR^2}{x_{1n}^2(x_{1n}^2-2)}\left[\frac{\mid\nabla\Omega_{2-}\mid^2(\Omega_0-\omega)}{D^2x_{1n}^4R^{-4}+(\Omega_0-\omega)^2}+\frac{\mid\nabla\Omega_{2+}\mid^2(\Omega_0+\omega)}{D^2x_{1n}^4R^{-4}+(\Omega_0+\omega)^2}\right]+\frac{M}{2}\left[\frac{\mid\Omega_{2+}\mid^2}{\Omega_0+\omega}+\frac{\mid\Omega_{2-}\mid^2}{\Omega_0-\omega}\right].\end{aligned} \tag{26}$$

Here $\mathbf{\Omega}_2$, $\nabla\mathbf{\Omega}_2$, and $\nabla\mathbf{\Omega}_1$ are evaluated at the center of the cell and $\Omega_{2\pm}=\Omega_{2x}\pm i\Omega_{2y}$. The last term in (26) is a Bloch-Siegert shift,[10] which has no analog in Eq. (56) of CSH since $\mathbf{\Omega}_1(0)=0$ by definition.

The last three terms in (25) represent the relaxation due to virtual emission and absorption of σ_+, π, and σ_- photons from the oscillating magnetic field. A $\sigma_\pm$ photon carries ± 1 unit of angular momentum along the z axis, and a π photon carries no angular momentum along the z axis. The relative densities of $\sigma_\pm$ and π photons are proportional to $\frac{1}{2}\mid\Omega_{2\pm}\mid^2$ and $\mid\Omega_{2z}\mid^2$. When a σ_+ photon is absorbed by spin in the uniform mode, the energy of the photon field decreases by $\hbar\omega$ and the energy of the spin increases by $\hbar\Omega_0-i\hbar Dx_{1n}^2/R^2$. The imaginary part of the spin energy comes from the natural lifetime $R^2D^{-1}x_{1n}^{-2}$ of a spin in the diffusion mode ($1\mu n$). The total change in the energy of the photons and the spins is therefore

$$\hbar(\Omega_0-\omega)-i\hbar Dx_{1n}^2/r^2\ , \tag{27}$$

and this is a representative "energy denominator" of the second or third line in (21). Note that the Bloch-Siegert shift comes from terms in (21) with purely imaginary denominators, that is, from virtual transitions with no change in the diffusional state. Consequently, there is no relaxation associated with the Bloch-Siegert shift.

The limits of validity of these calculations are the same as those discussed in CSH if $\mathbf{\Omega}_2(0)=0$ and there is no Bloch-Siegert shift. If the mean value $\mathbf{\Omega}_2(0)$ is nonzero, we must also have

$$\mid\Omega_0\pm\omega\mid\ \gg\ \mid\Omega_2\mid\ . \tag{28}$$

A. Relaxation during magnetic resonance

As an application of the results derived above we will discuss relaxation during magnetic resonance. The fre-

quency ω of the oscillating field will be close to the resonant frequency, that is, $|\omega| \approx |\Omega_0|$. Since the oscillating field is supposed to induce transitions between the spin sublevels, it will also have a nonzero spatially averaged value $\Omega_2(0)$ so the condition (28) will be violated. To avoid the difficulties associated with the violation of (28) we will discuss the behavior of the spins in the rotating coordinate system[11] where the spin-density matrix can be written as

$$|\sigma) = e^{i\omega t L_z} |\rho) \ . \tag{29}$$

Recall that one can use either $|\rho)$ or $|\sigma)$ to calculate the expectation value of a vector observable, say, the nuclear spin $\langle \mathbf{K} \rangle$ of the atoms. The prescription is

$$\begin{aligned} \langle \mathbf{K} \rangle &= (\mathbf{K}|\rho) = (\tilde{\mathbf{K}}|\sigma) \\ &= \tilde{\mathbf{x}}(K_x|\sigma) + \tilde{\mathbf{y}}(K_y|\sigma) + \tilde{\mathbf{z}}(K_z|\sigma) \ , \end{aligned} \tag{30}$$

where we have used the notation $(\mathbf{K}|\rho) = \mathrm{Tr}[\mathbf{K}\rho]$, $(\tilde{\mathbf{K}}|\sigma) = \mathrm{Tr}[\tilde{\mathbf{K}},\sigma]$, etc. to denote expectation values in polarization space. We note that the expectation values in (30) are all understood to be evaluated at the same spatial position $\mathbf{r}$ within the cell. The rotating unit vectors are

$$\begin{aligned} \tilde{\mathbf{x}} &= \mathbf{x}\cos\omega t + \mathbf{y}\sin\omega t \ , \\ \tilde{\mathbf{y}} &= -\mathbf{x}\sin\omega t + \mathbf{y}\cos\omega t \ , \\ \tilde{\mathbf{z}} &= \mathbf{z} \ . \end{aligned} \tag{31}$$

Thus (30) implies that the expectation values $(K_x|\sigma)$ and $(K_y|\sigma)$ are the projections of $\langle \mathbf{K} \rangle$ on the rotating vectors $\tilde{\mathbf{x}}$ and $\tilde{\mathbf{y}}$.

Differentiating (29) with respect to time and making use of (10) we find $|\sigma)$ obeys an evolution equation analogous to the evolution equation (10) for $|\rho)$,

$$\begin{aligned} \frac{\partial}{\partial t}|\sigma) &= i\omega L_z|\sigma) + e^{i\omega t L_z}\frac{\partial}{\partial t}|\rho) \\ &= (-i\boldsymbol{\Omega}_r\cdot\mathbf{L} + D\nabla^2)|\sigma) \ . \end{aligned} \tag{32}$$

Equation (32) describes spins which diffuse through the gas and simultaneously rotate at the effective Larmor frequency $\boldsymbol{\Omega}_r$. It can be solved by the perturbative methods discussed in the preceding section. From inspection of (32), (9), and (10) and from the fact that

$$e^{i\omega t L_z} L_\pm e^{-i\omega t L_z} = e^{\pm i\omega t} L_\pm \tag{33}$$

and

$$e^{i\omega t L_z} L_z e^{-i\omega t L_z} = L_z \ , \tag{34}$$

we find that $\boldsymbol{\Omega}_r$ can be written as the sum of four components

$$\boldsymbol{\Omega}_r = \boldsymbol{\Omega}_a + \boldsymbol{\Omega}_b + \boldsymbol{\Omega}_c + \boldsymbol{\Omega}_d \ . \tag{35}$$

The homogeneous, static component is

$$\boldsymbol{\Omega}_a = \tfrac{1}{2}[(\mathbf{x}+i\mathbf{y})\Omega_{2-} + \mathbf{z}(\Omega_0-\omega)] + \text{c.c.} \ , \tag{36}$$

where c.c. denotes the complex conjugate of the preceding expression. The homogeneous, oscillating component is

$$\boldsymbol{\Omega}_b = [\tfrac{1}{2}(\mathbf{x}-i\mathbf{y})\Omega_{2+}e^{-2i\omega t} + \mathbf{z}\Omega_{2z}e^{-i\omega t}] + \text{c.c.} \tag{37}$$

The homogeneous oscillating component $\boldsymbol{\Omega}_b$ can cause Bloch-Siegert shifts[10] similar to those discussed in connection with (23), and it can also lead to various parametric resonance phenomena,[12–14] but it cannot cause spin relaxation, so we will not consider it in more detail. The inhomogeneous, static component is

$$\boldsymbol{\Omega}_c = \mathbf{r}\cdot\nabla\tfrac{1}{2}[(\mathbf{x}+i\mathbf{y})\Omega_{2-} + \mathbf{z}\Omega_{1z}] + \text{c.c.} \tag{38}$$

The inhomogeneous, oscillating component is

$$\begin{aligned} \boldsymbol{\Omega}_d = \mathbf{r}\cdot\nabla[&\tfrac{1}{2}(\mathbf{x}-i\mathbf{y})(\Omega_{2+}e^{-2i\omega t} + \Omega_{1+}e^{-i\omega t}) \\ &+ \mathbf{z}\Omega_{2z}e^{-i\omega t}] + \text{c.c.} \end{aligned} \tag{39}$$

By comparing (1) and (36) we note that it is possible to write

$$\boldsymbol{\Omega}_a = \frac{\lambda}{2}[\mathbf{B}_2'\cdot(\mathbf{x}\mathbf{x}+\mathbf{z}\mathbf{z}) + \mathbf{B}_2''\times\mathbf{z}] + \lambda\mathbf{B}_0 - \omega\mathbf{z} \ , \tag{40}$$

where the in-phase field component $\mathbf{B}_2'$ and the quadrature component $\mathbf{B}_2''$ were defined in (1). Similarly, we can write

$$\boldsymbol{\Omega}_c = \lambda\mathbf{r}\cdot\nabla\{\tfrac{1}{2}[\mathbf{B}_2'\cdot(\mathbf{x}\mathbf{x}+\mathbf{y}\mathbf{y}) + \mathbf{B}_2''\times\mathbf{z}] + B_{1z}\mathbf{z}\} \ . \tag{41}$$

The Larmor frequencies $\boldsymbol{\Omega}$, the fields $\mathbf{B}$, and their gradients $\nabla\boldsymbol{\Omega}$ and $\nabla\mathbf{B}$, which occur on the right-hand sides of (36)–(41), are to be evaluated at the center of the cell where $\mathbf{r}=0$.

We define the Rabi frequency ω_r by

$$\omega_r = |\Omega_{a\pm}| = |\Omega_{2-}| \ . \tag{42}$$

Then, as illustrated in Fig. 1, (36) becomes

$$\boldsymbol{\Omega}_a = \Omega_a\mathbf{w} \ , \tag{43}$$

where

$$\Omega_a = [(\Omega_0-\omega)^2 + \omega_r^2]^{1/2} \ . \tag{44}$$

The axis of quantization $\mathbf{w}$ is

$$\mathbf{w} = \mathbf{x}\cos\alpha\sin\beta + \mathbf{y}\sin\alpha\sin\beta + \mathbf{z}\cos\beta \ . \tag{45}$$

The colatitude angle of $\mathbf{w}$ is

$$\beta = \tan^{-1}\frac{\omega_r}{\Omega_0-\omega} \ , \tag{46}$$

and the azimuthal angle is

$$\alpha = \tan^{-1}\frac{\Omega_{ay}}{\Omega_{ax}} = \tan^{-1}\frac{B_{2y}'-B_{2x}''}{B_{2x}'+B_{2y}''} \ . \tag{47}$$

We may imagine that the $\mathbf{w}$ axis was formed by rotating the $\mathbf{z}$ axis by the angle β about the axis

$$\mathbf{v} = \mathbf{y}\cos\alpha - \mathbf{x}\sin\alpha \ , \tag{48}$$

and we may obtain a complete set of Cartesian unit vectors $(\mathbf{u},\mathbf{v},\mathbf{w})$ by defining

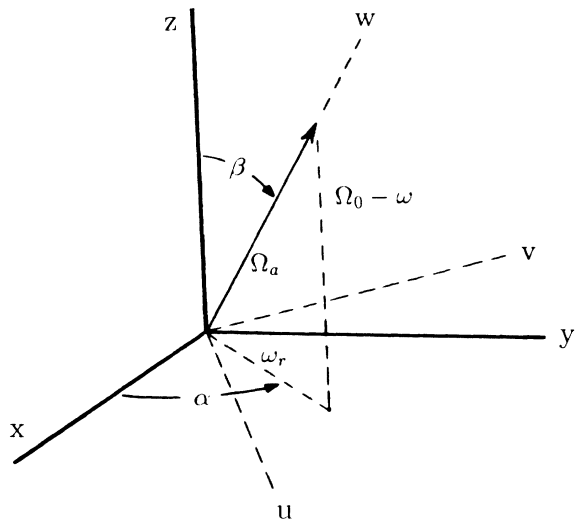

FIG. 1. Quantization axes **u**, **v**, and **w** for the density matrix $|\sigma)$. The spin expectation value $(\mathbf{K}|\sigma)$ rotates about the axis **w** at the frequency Ω_a, which can be determined from the static and oscillating magnetic fields with (40). According to (30), the expectation value of the spin, as viewed from the laboratory system at the same spatial location **r**, is $\langle\mathbf{K}\rangle=(\bar{\mathbf{x}}\mathbf{x}+\bar{\mathbf{y}}\mathbf{y}+\bar{\mathbf{z}}\mathbf{z})\cdot(\mathbf{K}|\sigma)$. Thus, in comparison to $(\mathbf{K}|\sigma)$, $\langle\mathbf{K}\rangle$ has an additional rotational velocity ω about the z axis. For this reason $(\mathbf{K}|\sigma)$ is called the expectation value of the spin in the rotating coordinate system, and (32) is said to describe the evolution of the spin polarization in the rotating coordinate system.

$$\mathbf{u}=\mathbf{v}\times\mathbf{w}=\mathbf{x}\cos\alpha\cos\beta+\mathbf{y}\sin\alpha\cos\beta-\mathbf{z}\sin\beta\ . \tag{49}$$

The criterion (28) now becomes

$$|\Omega_a\pm2\omega|\gg|\Omega_{2+}|\ ,\quad |\Omega_a\pm\omega|\gg|\Omega_{2z}|\ , \tag{50}$$

and this will be satisfied for most magnetic resonance experiments. We can therefore use (25) and (26) to describe the relaxation due to field inhomogeneities in the rotating coordinate system. There will be an effectively static inhomogeneity $\nabla\Omega_c$ which we identify with $\nabla\Omega_1$, there will be an oscillating, homogeneous field Ω_b which causes a Bloch-Siegert shift such as that due to Ω_2 in the last term of (26), and there will be inhomogeneities $\nabla\Omega_d$ oscillating at the frequencies ω and 2ω, which we can identify with the inhomogeneity $\nabla\Omega_2$ of (25) and (26).

It is frequently the case that the oscillation frequency ω satisfies the conditions

$$\omega^2\gg\Omega_a^2,\quad \omega^2\gg D^2R^{-4}\ . \tag{51}$$

If the condition (51) holds, which we shall assume to be the case henceforth, the relaxation [described by the last three terms of (25)] due to the effectively oscillating field inhomogeneity Ω_d is negligible compared to the relaxation [described by the first two terms of (25)] caused by the effectively static field inhomogeneity Ω_c.

To calculate the relaxation due to the effectively static field inhomogeneity (38), we need only make the replacement $\Omega_{1x}\rightarrow\Omega_{cu}$, $\Omega_{1y}\rightarrow\Omega_{cv}$, $\Omega_{1z}\rightarrow\Omega_{cw}$, and $\Omega_0\rightarrow\Omega_a$ in (25) and (26). From (38) and (45), (48) and (49) we find

$$\Omega_{cu}=\Omega_c\cdot\mathbf{u}=\mathbf{r}\cdot\nabla(\cos\alpha\cos\beta\Omega_{2x}+\sin\alpha\cos\beta\Omega_{2y}-\sin\beta\Omega_{1z})\ , \tag{52}$$

$$\Omega_{cv}=\Omega_c\cdot\mathbf{v}=\mathbf{r}\cdot\nabla(\cos\alpha\Omega_{2y}-\sin\alpha\Omega_{2x})\ , \tag{53}$$

$$\Omega_{cw}=\Omega_c\cdot\mathbf{w}=\mathbf{r}\cdot\nabla(\cos\alpha\sin\beta\Omega_{2x}+\sin\alpha\sin\beta\Omega_{2y}+\cos\beta\Omega_{1z})\ . \tag{54}$$

Substituting the appropriate gradients into (25) we find

$$\mathcal{R}\gamma^{(2)}_{0,LM}=\frac{8M^2R^4}{175D}|\nabla\Omega_{cw}|^2+\sum_n\frac{D[L(L+1)-M^2]}{(x_{1n}^2-2)}\times\left[\frac{|\nabla\Omega_{cu}|^2+|\nabla\Omega_{cv}|^2}{D^2x_{1n}^4R^{-4}+\omega_r^2+(\Omega_0-\omega)^2}\right]\ . \tag{55}$$

The polarization quantum numbers L and M in (55) refer to the w axis of Fig. 1.

Suppose that we can neglect the inhomogeneity of the oscillating field Ω_2 so the relaxation is due solely to the inhomogeneous static field Ω_1. Then (55) implies that the longitudinal relaxation rate in the rotating coordinate system is

$$\frac{1}{T_{r1}}=\mathcal{R}\gamma^{(2)}_{0,10}=\gamma_1 g(r,s)\ . \tag{56}$$

Similarly, the transverse relaxation rate is

$$\frac{1}{T_{r2}}=\mathcal{R}\gamma^{(2)}_{0,11}=\gamma_1\left[\frac{g(r,s)}{2}+\frac{s^2}{1+s^2}\right]\ . \tag{57}$$

We have written $1/T_{r1}$ and $1/T_{r2}$ in terms of the characteristic relaxation rate

$$\gamma_1=\frac{8R^4|\nabla\Omega_{1z}|^2}{175D}\ , \tag{58}$$

which is the high-pressure limit of the transverse relaxation rate in the laboratory system, as discussed in connection with Eq. (61) of CSH.

The line-shape function is

$$g(r,s)=\sum_n\frac{175}{4(x_{1n}^2-2)(x_{1n}^4+r^2+r^2s^2)(1+s^2)}\ . \tag{59}$$

The relative Rabi frequency r, which is analogous to the relative pressure p/p^* of Eq. (2) of CSH, is

$$r=\frac{\omega_rR^2}{D}\ . \tag{60}$$

The relative detuning, the ratio of the detuning frequency $\Omega_0-\omega$ to the Rabi frequency ω_r, is

$$s=\frac{(\Omega_0-\omega)}{\omega_r}\ . \tag{61}$$

The relaxation rates $1/T_{r1}$ and $1/T_{r2}$ are sketched in Fig. 2 for several values of r. We note that the longitudinal relaxation rate is peaked at resonance, and the transverse relaxation rate is at a minimum at resonance. At exact

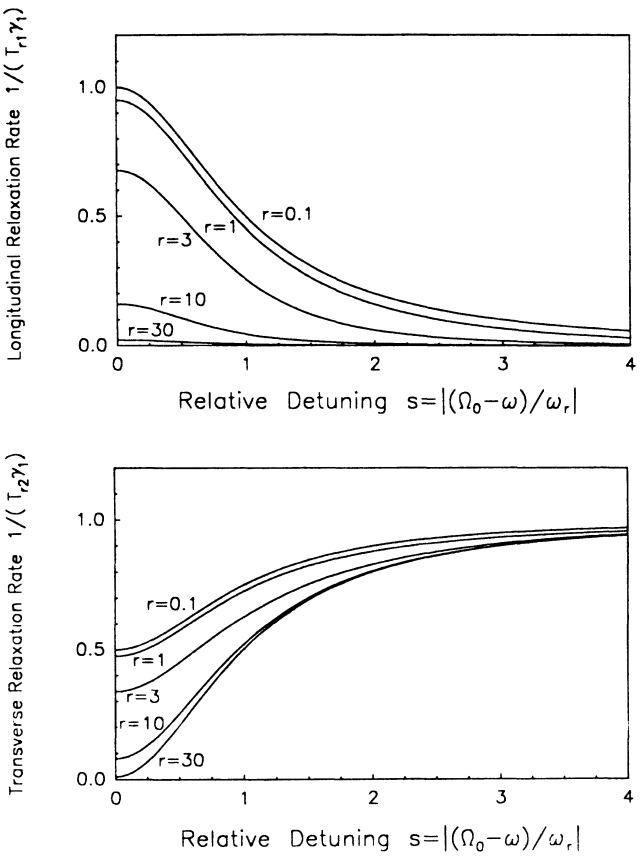

FIG. 2. Relaxation rates in the rotating coordinate system due to inhomogeneities in the static field. The rates are calculated according to (56) and (57) when there is negligible relaxation due to the inhomogeneity $\nabla\Omega_2$.

resonance $T_{r2}=2T_{r1}$. When the frequency is well off resonance, $T_{r2}\ll T_{r1}$.

III. EXPERIMENTAL STUDIES

We have performed experiments to check the validity of the theory. The basic geometry of the apparatus is shown in Fig. 3. We used spherical Pyrex glass cells containing 1 Torr of xenon, isotopically enriched to 69% ^{129}Xe, and about 25 Torr of nitrogen gas, which is the main species which limits the diffusion rate of the xenon atoms. The pressures are quoted for a cell-filling temperature of 25° C. The cells also contain several milligrams of rubidium metal of natural isotopic composition. At the beginning of each experiment, the Rb atoms in the vapor phase were maintained at high polarization by optically pumping with several hundred milliwatts of circularly polarized 7948-Å light from a cw dye laser, pumped by a krypton-ion laser. During this pumping phase, which took several minutes, angular momentum was transferred from the spin polarized Rb atoms into the nuclear spins of the ^{129}Xe atoms by spin exchange collisions in van der Waals molecules.[15–18] Once the nuclei had been polarized, the laser light was blocked and the mirror of Fig. 3 was removed to allow unpolarized 7948-Å D_1 light from a Rb resonance lamp to pass through the cell, through a photoelastic modulator and onto a silicon photodiode. The photoelastic modulator was used to detect the small amount of circular polarization, which was proportional to the longitudinal nuclear spin $\langle K_z\rangle$ of the ^{129}Xe atoms. More details about the detection process can be found in the work of Zeng *et al.*[18]

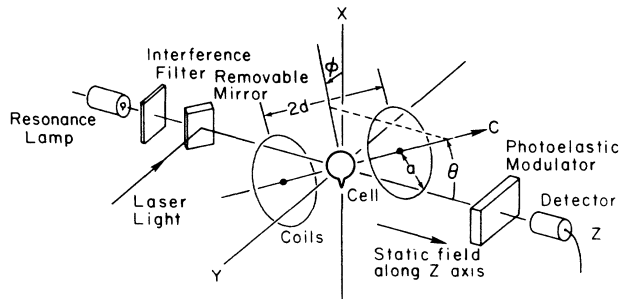

FIG. 3. The most important optical parts of the apparatus used to study the effect of magnetic field inhomogeneities on nuclear-spin-relaxation rates. Two or more pairs of magnetic field coils were used in the experiments, and one pair is shown to illustrate the polar angles θ and ϕ of the symmetry axis.

A convenient way to create magnetic fields is to use a pair of identical coaxial coils, each having n circular turns of wire carrying a current I. The radius of the coils is a and they are separated by a distance $2d$ as sketched in Fig. 3. The coils are aligned along the direction of the unit vector $\mathbf{c}$. Several coils such as those shown in Fig. 3 were used simultaneously in the experiments to be described below. If homogeneous static or oscillating fields were needed, the coils were wired so that their fields added at the center of symmetry (the center of the cell of Fig. 3), and the coils were located as nearly as possible to the Helmholtz configuration where $2d=a$. The field from these Helmholtz coils was very homogeneous over the volume of the cell.

If known field inhomogeneities were needed, the coils were wired in opposition so that their fields canceled at the center of symmetry of the "inhomogeneity coils." At the center of the cell, the coils produce a magnetic field gradient which can be expressed in dyadic form as

$$\nabla\mathbf{B}(\mathbf{c})=\kappa I(3\mathbf{cc}-1)\ , \tag{62}$$

where the unit dyadic is $1=\mathbf{xx}+\mathbf{yy}+\mathbf{zz}$, and the calibration constant κ is

$$\kappa=\frac{3\pi na^2d}{5(d^2+a^2)^{5/2}}\,\mathrm{G\,cm\,A^{-1}}\ . \tag{63}$$

We can regard the gradient (62) as independent of position within the cell as long as the radius R of the cell is much smaller than the radius a of the coils. Let us describe the direction of $\mathbf{c}$ with the polar angles θ and ϕ as indicated in Fig. 3:

$$\mathbf{c}=\mathbf{x}\cos\phi\sin\theta+\mathbf{y}\sin\phi\sin\theta+\mathbf{z}\cos\theta\ . \tag{64}$$

Substituting (64) into (62) and taking matrix elements between the unit vectors $\mathbf{x}$, $\mathbf{y}$, and $\mathbf{z}$ we find that the matrix form of (62) is

$$\nabla\mathbf{B}(\mathbf{c})=\begin{bmatrix}\partial B_x/\partial x & \partial B_y/\partial x & \partial B_z/\partial x\\ \partial B_x/\partial y & \partial B_y/\partial y & \partial B_z/\partial y\\ \partial B_x/\partial z & \partial B_y/\partial z & \partial B_z/\partial z\end{bmatrix}$$
$$=3\kappa I\begin{bmatrix}\sin^2\theta\cos^2\phi-\frac{1}{3} & \sin^2\theta\sin\phi\cos\phi & \sin\theta\cos\theta\cos\phi\\ \sin^2\theta\sin\phi\cos\phi & \sin^2\theta\sin^2\phi-\frac{1}{3} & \sin\theta\cos\theta\sin\phi\\ \sin\theta\cos\theta\cos\phi & \sin\theta\cos\theta\sin\phi & \cos^2\theta-\frac{1}{3}\end{bmatrix}. \quad (65)$$

To aid in the discussion of the experiments we will write out explicitly several special cases of (65). For coils aligned along the x axis we have

$$\nabla\mathbf{B}(\mathbf{x})=\kappa I\begin{bmatrix}2 & 0 & 0\\ 0 & -1 & 0\\ 0 & 0 & -1\end{bmatrix}. \quad (66)$$

For coils aligned along the y axis we have

$$\nabla\mathbf{B}(\mathbf{y})=\kappa I\begin{bmatrix}-1 & 0 & 0\\ 0 & 2 & 0\\ 0 & 0 & -1\end{bmatrix}. \quad (67)$$

For coils aligned along the z axis we have

$$\nabla\mathbf{B}(\mathbf{z})=\kappa I\begin{bmatrix}-1 & 0 & 0\\ 0 & -1 & 0\\ 0 & 0 & 2\end{bmatrix}. \quad (68)$$

We may pass the same current I through two identical pairs of coils, aligned along the x axis and y axis, respectively, such that the total field gradient is

$$\nabla\mathbf{B}(\mathbf{x})-\nabla\mathbf{B}(\mathbf{y})=\kappa I\begin{bmatrix}3 & 0 & 0\\ 0 & -3 & 0\\ 0 & 0 & 0\end{bmatrix}. \quad (69)$$

Note that the third row of the field gradient (69) is zero. It will also be convenient to orient the coil axis $\mathbf{c}$ at the "magnetic angle" $\theta_m=\cos^{-1}1/\sqrt{3}=54.7°$. For $\theta=\theta_m$ and $\phi=0$ we have from (65)

$$\nabla\mathbf{B}(\theta_m,0)=\kappa I\begin{bmatrix}1 & 0 & \sqrt{2}\\ 0 & -1 & 0\\ \sqrt{2} & 0 & 0\end{bmatrix}. \quad (70)$$

Similarly, for $\theta=\theta_m$ and $\phi=\pi/2$ we have

$$\nabla\mathbf{B}(\theta_m,\pi/2)=\kappa I\begin{bmatrix}-1 & 0 & 0\\ 0 & 1 & \sqrt{2}\\ 0 & \sqrt{2} & 0\end{bmatrix}. \quad (71)$$

A. Components of ∇B which cause relaxation

To test which parts of the gradient tensor are important in causing relaxation, we have carried out a set of measurements to study $1/T_{r2}$ for the field gradients (66) and (69). After being polarized as described above, the ^{129}Xe nuclei were subjected to a resonant, homogeneous, oscillating magnetic field while a static magnetic field inhomogeneity was created by passing constant currents through one or more pairs of inhomogeneity coils. The basic parts of the apparatus are shown in Fig. 3. We made no attempt to shield the magnetic noise in the laboratory and this added a small amount of scatter to the experimental data. The detected signal is proportional to the projection of the nuclear spin onto the z axis.[18] The magnetic field that the atoms experience in the rotating frame can be understood with reference to Fig. 1. When the oscillating magnetic field is on resonance we have $\beta=\pi/2$ and the axis of quantization $\mathbf{w}$ in the rotating frame is perpendicular to the z axis. The spin polarization rotates at the Rabi frequency $\Omega_a=\omega_r$ about the w axis and is alternately parallel and antiparallel to the z axis. The polarization in the rotating frame will be purely transverse and it will decay at the rate $1/T_{r2}$. The curve labeled $s=0$ in Fig. 4(a) is a representative piece of experimental data. The envelope of the transient is well represented by a decaying exponential curve of the form $\exp(-t/T_{r2})$.

The results of many measurements of T_{r2} are shown in Fig. 5. The closed triangles of Fig. 5 were taken as a function of the current I in coils which produced the gradient (69). The measurements are plotted as a function of $3\kappa I$ which is the increment to the ambient value of $\partial B_x/\partial x$ or the decrement to $\partial B_y/\partial y$. Since the gradient tensor (69) has $\nabla B_z=0$, we would expect inhomogeneity coils to cause no relaxation, according to (58), and none was observed. The "theoretical" line for the closed triangles of Fig. 5 is simply a least-squares fit of a horizontal line.

The closed circles of Fig. 5 were taken as a function of the current I in coils which produced the gradient (66). The measurements are plotted as a function of κI which is the decrement to the ambient value of $\partial B_z/\partial z$. According to (57) the contribution to the relaxation rate from field inhomogeneities should be

$$\frac{1}{T_{r2}}=\frac{\gamma_1 g(r,0)}{2}$$
$$=\frac{4R^4\lambda^2 g(r,0)}{175D}(|\partial B_{1z}/\partial x|^2+|\partial B_{1z}/\partial y|^2+|\partial B_{1z}/\partial z-\kappa I|^2), \quad (72)$$

where

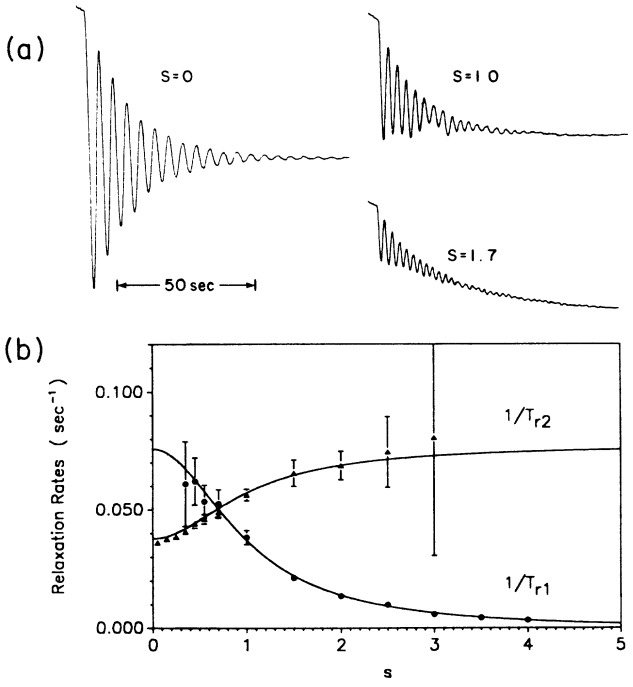

FIG. 4. (a) Spin relaxation of ^{129}Xe due to magnetic field inhomogeneities. Traces are shown for three values of the detuning parameter $s=(\Omega_0-\omega)/\omega_r$. For clarity, the decay rates were increased by applying a large gradient described by (71). The envelopes of the transients decay at the rate $1/T_{r2}+1/T$ and the center lines decay at the rate $1/T_{r1}+1/T$, where $1/T_{r1}$ and $1/T_{r2}$ should be given by (56) and (57), and $1/T$ is a small contribution to the relaxation due to collisions of ^{129}Xe atoms with Rb atoms and with the cell walls. The most reliable data for T_{r2} are obtained for $s\leq 1$ and the most reliable data for T_{r1} are obtained for $s\geq 1$. (b) Values of T_{r1} and T_{r2}, extracted from traces of the sort shown above, but with a smaller gradient (66), are plotted as a function of s. The solid lines are best fits to the data of the functions (56) and (57). A more detailed discussion of these data is contained in Sec. III B.

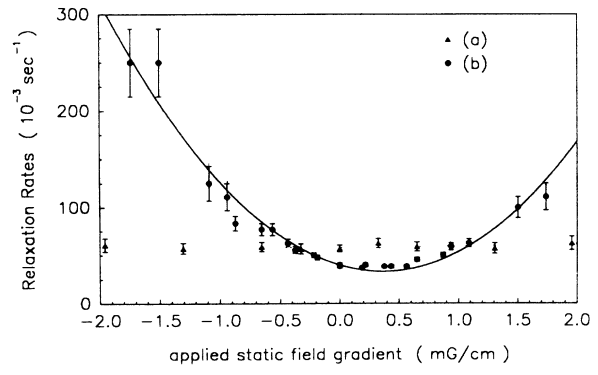

FIG. 5. Transverse relaxation rate T_{r2} in the rotating frame, as a function of field gradient. (a) The relaxation produced by a current I in coils which produce the gradient (69) as a function of $3\kappa I$. The inhomogeneity coils have no effect on ∇B_z. (b) The relaxation produced by a current I in coils which produce the gradient (66) as a function of κI. The inhomogeneity coils do contribute to ∇B_z. These data show that spin relaxation during magnetic resonance is dominated by ∇B_z and that the remaining independent parts of the gradient tensor, for example, $\partial B_x/\partial x$, have relatively little effect on the relaxation rate.

$$\lambda=\frac{g_K\mu_B}{\hbar}=7400\ \text{sec}^{-1}\,\text{G}^{-1} \tag{73}$$

is the gyromagnetic ratio of ^{129}Xe nuclei. In (72) we have written the field gradient as the sum of an ambient part ∇B_{1z} and an applied part $\nabla B_z(\mathbf{x})=(0,0,-\kappa I)$ given by (66). The ambient components are largely due to steel structures (cabinets, reinforced concrete) near the apparatus. The solid curve in Fig. 5 is the parabola

$$\frac{1}{T_{r2}}=(5.0\times 10^4)\ \text{sec}^{-1}\,\text{cm}^2\,\text{G}^{-2}$$
$$\times[(360\ \mu\text{G}\,\text{cm}^{-1})-\kappa I]^2+0.032\ \text{sec}^{-1}\ . \tag{74}$$

The ambient field $\partial B_{1z}/\partial z=360\ \mu\text{G}\,\text{cm}^{-1}$ and the minimum relaxation rate 0.032 sec^{-1} of the parabola (74) were obtained by a least-squares fit to the experimental data points of Fig. 5. The Rabi frequency of the experiments depicted in Fig. 5 was $\omega_r=6.28$ sec^{-1}, the effective radius of the cell was 0.60 cm, and the diffusion constant was $D=D_0(760/24.5)=3.4$ cm^2 sec^{-1}. The diffusion constant $D_0=0.11$ cm^2 sec^{-1} at 1 atm was determined in the experiments discussed in Sec. III C. The parameter r of (60) was therefore $r=0.67$, and we may evaluate (59) to find that $g(0.67,0)=0.97$. These parameters, along with the gyromagnetic ratio (73) were substituted into the expression $4R^4\lambda^2 g(r,0)/(175D)$ which, according to (72), should give the coefficient for the quadratic term of the parabola. The agreement with experiment is seen to be quite good.

The data of Fig. 5 illustrate clearly that spin relaxation during magnetic resonance is due mainly to ∇B_z and is little affected by $\partial B_x/\partial y=\partial B_y/\partial x$, $\partial B_x/\partial z$, and $\partial B_y/\partial y$. We can use coils which produce the gradients (70), (71), and (68) to cancel out $\partial B_z/\partial x$, $\partial B_x/\partial y$, and $\partial B_z/\partial z$, respectively, and to eliminate most of the relaxation due to field inhomogeneities in magnetic resonance experiments.

We note that all of the data of Fig. 5(b) were taken with constant currents in two pairs of coils which produced the gradients (70) and (68). The currents in these coils were set to minimize the relaxation rate, presumably by canceling out the elements $\partial B_z/\partial x=\partial B_x/\partial z$ and $\partial B_z/\partial z$ of the ambient gradient tensor.

B. Effects of detuning on relaxation

We also studied spin relaxation as a function of detuning from the Larmor frequency Ω_0 during magnetic resonance conditions. The sample cell was the same as the one discussed in Sec. III A, the pumping and probing procedures were the same, but the magnetic fields were more carefully controlled in these experiments. A static magnetic field was provided by a solenoid, and an oscillating field was provided by a pair of Helmholtz coils aligned with the y axis. A static gradient (66) was produced by passing a current $I=3.0$ mA through a pair of inhomogeneity coils aligned with the x axis. The coils had $n=4$ turns, a radius $a=1.70$ cm, and a spacing $2d=4.32$ cm. From (66) and (63) we conclude that

$\kappa=0.30\ \mathrm{G\,cm^{-1}\,A^{-1}}$. The important element of the gradient was $\partial B_z/\partial z=-\kappa I=-9.0\times10^{-4}\ \mathrm{G\,cm^{-1}}$. Two layers of μ metal shielded the cell from external magnetic noise, and an active feedback system eliminated long-term drifts of the magnetic field. With the exception of the inhomogeneity coils, the apparatus is exactly that described by Wu *et al.*[19]

At the end of the pump phase of the experiment and just before the oscillating field was turned on, the spin polarization of the ^{129}Xe nuclei was $\langle\mathbf{K}\rangle=P\mathbf{z}$, where the initial polarization amplitude P depended on how long the sample was pumped, the relaxation mechanisms in the cell, etc. At the instant the oscillating field was applied, the longitudinal spin polarization in the rotating coordinate system was $\mathbf{w}P\cos\beta$ and the transverse spin polarization was $-\mathbf{u}P\sin\beta$. The transverse polarization rotated about the w axis at the frequency Ω_a and decayed exponentially at the rate $1/T'_{r2}$. The longitudinal polarization in the rotating system decayed at the rate $1/T'_{r1}$. The signals observed with the apparatus of Fig. 3 were proportional to the projection of the nuclear-spin polarization onto the z axis, and they were therefore of the form

$$S(t)=AP(e^{-t/T'_{r2}}\sin^2\beta\cos\Omega_a t+e^{-t/T'_{r1}}\cos^2\beta)\ , \tag{75}$$

where A is a proportionality constant. Representative transients for three values of s, the detuning parameter defined in (61), are shown in Fig. 4(a). The envelopes of the transients decay at the rate $1/T'_{r2}=1/T_{r2}+1/T$ and the centerlines decay at the rate $1/T'_{r1}=1/T_{r1}+1/T$, where $1/T_{r1}$ and $1/T_{r2}$ should be given by (56) and (57), and $1/T$ is relaxation, typically about 30% of $1/T'_{r2}$, which is due to causes other than inhomogeneities. Collisions of ^{129}Xe atoms with Rb atoms and with the walls are the main contributors to $1/T$, which can be determined measuring $1/T'_{r1}$ at very large detunings where field inhomogeneities have a negligible effect on the relaxation rates. We subtracted $1/T$ from the raw experimental data to obtain the values for $1/T_{r1}$ and $1/T_{r2}$ plotted in Fig. 4. In agreement with the predictions of the theory, we measured the same relaxation rates, within experimental error, for $+|s|$ and $-|s|$, and the mean measured values for $\pm|s|$ are plotted in Fig. 4(b). We could determine s experimentally from the measured frequencies Ω_a of transients such as those of Fig. 4(a), and from the known absolute detunings $\Omega_0-\omega$. The values of T_{r1} and T_{r2} were fitted simultaneously by least squares to the functions (56) and (57) with the cell radius R as a free parameter. The best-fitting radius was $R=0.60$ cm, which is slightly smaller than our estimate $R=0.61$ cm based on measurements with calipers. At zero detuning, the data show that the longitudinal relaxation rate approaches a value which is twice that of the transverse relaxation rate, as predicted by (56) and (57).

C. Motional narrowing

A striking prediction of CSH is that at low relative pressures, motional narrowing occurs and $1/T_1$ is proportional to pressure. In contrast, the classical result,[2,3] valid at high relative pressure, predicts that $1/T_1$ is inversely proportional to pressure. It was shown in CSH that the transition from low-pressure behavior to high-pressure behavior occurs when the relative pressure

$$\frac{p}{p^*}=\frac{\Omega_0R^2}{D} \tag{76}$$

is on the order of 4. In practice, it is difficult to perform experiments in static magnetic fields at small values of the relative pressure. An experimentally convenient magnetic field for ^{129}Xe is $B_0=0.1$ G, where the Larmor frequency is $\Omega_0=\lambda B_0=740\ \mathrm{sec^{-1}}$. For cells such as those discussed above with a radius of $R=0.60$ cm, and $D\approx3.2\ \mathrm{cm^2\,sec^{-1}}$ at a pressure of $p\approx30$ Torr, the relative pressure is $p/p^*\approx86$. To get $p/p^*\approx1$ we would have to use a pressure of $p\approx\frac{30}{86}=0.35$ Torr, an impractically low value. As discussed by Zeng *et al.*,[18] the spin transfer efficiency from the optically pumped alkali atoms to the noble-gas nuclei drops to unusable values for pressures below about 10 Torr. Furthermore, it would not be possible to optically pump the alkali vapor efficiently at such low pressures because of the rapid diffusion of the spin polarized alkali atoms to the cell walls. One could also think of decreasing p/p^* by decreasing the cell radius R, but we would have to decrease R by $\sqrt{86}=9.3$ to get $p/p^*=1$, and the resulting cells would have to have radii of 0.6 mm or less, an impractically small value. Making a series of cells with different radii or different pressures is not an attractive option because of the difficulty of controlling the experimental parameters of many different cells and the need to interchange them in the experimental apparatus. It would be much better to use a single cell mounted permanently in the apparatus, and to vary p/p^* by changing the magnitude of the Larmor frequency Ω_0. To ensure that $p/p^*\le1$ in the sample cells discussed above, where $R=0.60$ cm, we would need a Larmor frequency $\Omega_0\le2\pi\times1.4$ Hz, which corresponds to a static field of about 10^{-3} G. It is very difficult to produce such small static magnetic fields with the required stability of magnitude and direction.

A more practical way[20] to study relaxation caused by magnetic field inhomogeneities under motional narrowing conditions is to work in the rotating coordinate system. At exact resonance, when $\omega=\Omega_0$, the longitudinal relaxation rate $1/T_{r1}$ in the rotating coordinate system, given by (56), depends on relative Rabi frequency r in the same way as the longitudinal relaxation rate $1/T_1$ in the laboratory system, given by Eq. (55) of CSH, depends on the relative pressure p/p^*. It is relatively easy to produce a very small and stable *rotating* magnetic field, and we already pointed out that the relative Rabi frequency for the data of Fig. 4(b) was $r\approx0.7$, that is, the data were taken well into the motional narrowing regime. By combining experiments in the rotating system with experiments in the laboratory system, we have measured longitudinal relaxation rates over a domain which includes both high and low relative pressures, that is, from $r=0.4$ to $p/p^*=98$.

All measurements were done with the same apparatus described in Sec. III B. The sample cell differed slightly from that of Secs. III A and III B. The cell had a nomi-

nal radius, based on measurements with calipers, of $R=0.55$ cm. It contained 30.5 Torr of N_2 gas and 1 Torr xenon, isotopically enriched to 69% ^{129}Xe.

To study the spin-relaxation rates at high relative pressures, we observed the longitudinal spin relaxation in the laboratory frame. The spins were subject to a homogeneous static field which produced a Larmor frequency Ω_0 and to an inhomogeneous static field described by (66). The inhomogeneity coils were the same as in Sec. III B but the coil spacing was larger, $2d=5.8$ cm. The calibration factor (63) of the coils was $\kappa=0.147$ G cm^{-1} A^{-1}. At 8.2-sec intervals the spins were inverted with a π pulse, as discussed in more detail below, to eliminate the effects of slow drifts in the overall gain of the recording system. A representative relaxation transient is shown in Fig. 6. Measurements were made at values of the static magnetic field B_0 ranging from 0.11 to 0.02 G. The corresponding values of p/p^* ranged from 17 to 91. At each value of the static field, relaxation transients such as that of Fig. 6 were measured for several values of the applied field inhomogeneity, corresponding to static currents I of 6–50 mA in the inhomogeneity coils. To facilitate comparison of these experiments with theory we have converted the measured values of the relaxation rates to experimental reduced rates $1/\tau_1$ defined by

$$\frac{1}{\tau_1}=\frac{1}{\gamma_0 T_1} , \tag{77}$$

where the characteristic rate γ_0, as defined in Fig. 1 of CSH, is

$$\gamma_0=\frac{(|\nabla\Omega_{1x}|^2+|\nabla\Omega_{1y}|^2)R^2}{\Omega_0}=\frac{5(\lambda\kappa RI)^2}{\Omega_0} . \tag{78}$$

According to Eq. (57) of CSH, the reduced rate, which is plotted as a function of p/p^* in Fig. 1 of CSH, should be equal to

$$\frac{1}{\tau_1}=\frac{8}{175}\frac{p}{p^*}g\left[\frac{p}{p^*},0\right] , \tag{79}$$

where the function $g(r,s)$ was defined by (59). For the high relative pressures of these experiments the theoretically predicted relaxation rate is very nearly equal to the classical value [Eq. (1) of CSH], that is, directly proportional to the diffusion constant D and independent of the cell radius. These data, plotted as the circular points in Fig. 7, are therefore ideal for the determination of D. By a least-squares fit of the data to the theory (79) with D as a free parameter we found that the diffusion constant of the cell was

$$D=2.7 \text{ cm}^2\text{ sec}^{-1} . \tag{80}$$

The total pressure in the cell was $p=31.5$ Torr, and the partial pressure of xenon was only 1 Torr. A reasonable estimate of the standard diffusion constant D_0 of xenon atoms in 1 atm of nitrogen gas is therefore

$$D_0=D\frac{p}{760\text{ Torr}}=0.11\text{ cm}^2\text{ sec}^{-1} . \tag{81}$$

This seems to be the first measurement of D_0 for xenon diffusing in nitrogen gas.

The experimental uncertainties were such that we do not claim a measurement accuracy any better than 30%. However, our experiments were not designed to measure diffusion constants, but to validate the new theory discussed in CSH and in this paper. It is clear that quantitative analysis of the nuclear-spin-relaxation rates of noble gases in the presence of known field inhomogeneities is an excellent new way to measure the diffusion constant of noble gases in various gaseous mixtures. Much more precise measurements could be made without much difficulty.

To study longitudinal spin relaxation at the equivalent of very low relative pressures, we carried out a series of

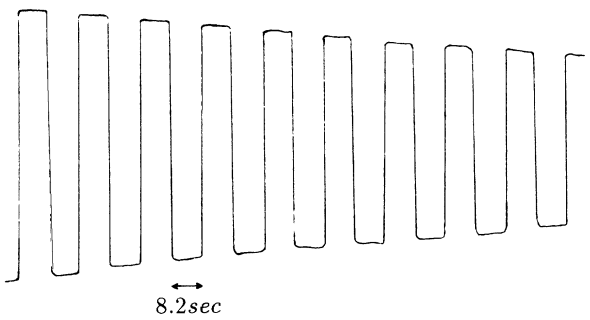

FIG. 6. A spin-relaxation transient for the decay of the longitudinal spin polarization in the laboratory system. Most of the relaxation is due to inhomogeneities of the static magnetic field. Slow drifts in the gain of the recording system were eliminated by using π pulses to invert the polarization from time to time. The open circles of Fig. 7 were obtained from transients such as this.

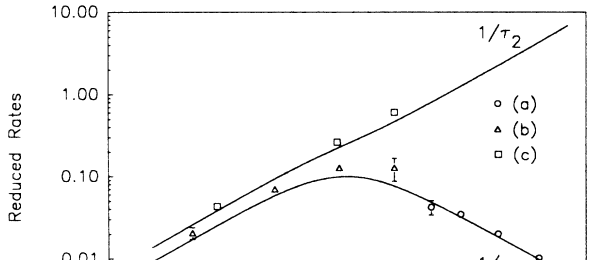

FIG. 7. (a) Open circles, measured values of the longitudinal relaxation rate $1/T_1$ of spins in the laboratory system in units of γ_0, defined by (78). The reduced rates $1/\gamma_0 T_1$ are plotted as a function of the reduced pressure p/p^* defined by (76). (b) Open triangles, measured values of the longitudinal relaxation rate $1/T_{r1}$ in the rotating coordinate system in units of γ_r, defined by (95). The reduced rates $1/\gamma_r T_{r1}$ are plotted as a function of $p/p^*=r$, where r is the relative Rabi frequency defined by (60). (c) Open squares, measured values of the transverse relaxation rate $1/T_{r2}$ in the rotating coordinate system in units of γ_r. The reduced rates $1/\gamma_r T_{r2}$ are plot d as a function of $p/p^*=r$. The solid lines are the theoretical curves (79) and (98).

experiments in the rotating coordinate system. The basic idea of these experiments was to orient the polarized spins along a small transverse magnetic field, rotating at the Larmor frequency, and to monitor the relaxation of the spins along this rotating quantization axis. Since our experimental procedure did not permit us to monitor transverse spin polarization in the laboratory frame, we had to periodically apply $\pi/2$ pulses of oscillating magnetic field to rotate the spins into alignment with the z axis, where the spin polarization could be measured. To facilitate the measurement, the spin polarization was also inverted with π pulses before being rotated back into alignment with the rotating magnetic field to permit more relaxation to occur. We used an inhomogeneous oscillating field to be sure that the theoretical predictions of the relaxation caused by this type of inhomogeneity were correct. Although these experiments were very instructive, they required the use of rather complicated sequences of pulses from two oscillators, one to provide the oscillating inhomogeneous field and one to provide the homogeneous quantizing field in the rotating coordinate system. One of the oscillators also provided π and $\pi/2$ pulses.

We began by polarizing the ^{129}Xe nuclei by spin exchange optical pumping, as described for the experiments above. In Fig. 8 we show representative data from the experiments, a simplified sketch of the apparatus is shown in Fig. 9, and an outline of the pulse sequences is shown in Fig. 10. Oscillating voltages were generated by two Hewlett-Packard 3325A function generators, which we call oscillators 1 and 2. These were tuned to the magnetic resonance frequency $\omega=\Omega_0$. The oscillators were ordinarily phase-locked together such that the phase of oscillator 1 led the phase of oscillator 2 by 90°. The oscillators drove voltage-to-current converters (not shown in Fig. 9) which could be connected to a pair of Helmholtz coils or to a pair of inhomogeneity coils in a sequence which was controlled by an Apple IIe computer.

Oscillating homogeneous fields were produced by currents in the Helmholtz coils, which had a symmetry axis along the y direction. These coils were wrapped on circular aluminum supports, and they were normally used to produce quasistatic fields for another experiment. At the oscillation frequencies (130 Hz) of these experiments, the Helmholtz coils acted like the primary of a transformer and the aluminum supports acted like a shorted secondary circuit. The currents induced in the coil supports caused the field at the cell to lag the driving current. Direct measurements with a pickup coil showed that the lag angle was $\chi=45°\pm5°$, as sketched in Fig. 10. There may also have been some small contributions to χ from eddy currents in nearby metal parts of the apparatus, but there was no evidence that the fields from the induced currents were inhomogeneous enough to

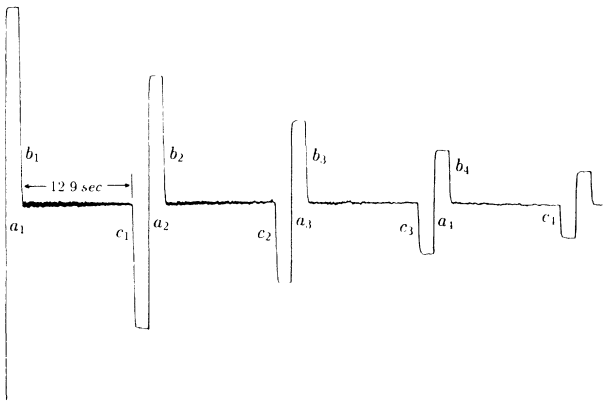

FIG. 8. Representative data for determining $1/T_{r1}$, the longitudinal relaxation rate in the rotating coordinate system. The initial spin polarization was oriented along the negative z axis. The spin polarization was inverted with a π pulse at the point a_1. At the point b_1 the spins were rotated with a $\pi/2$ pulse to orient them along the x axis. Between the points b_1 and c_1 the spins were subject to a homogeneous quantizing field along the x axis and to an inhomogeneous field which caused the spin polarization to relax at the rate $1/T_{r1}$. At the point c_1 the spins were rotated to orient them along the $-z$ axis of the rotating coordinate system. This sequence was repeated until the spin polarization was too small to measure. More details of the experimental procedure can be found in the discussion of Figs. 9 and 10 in the text.

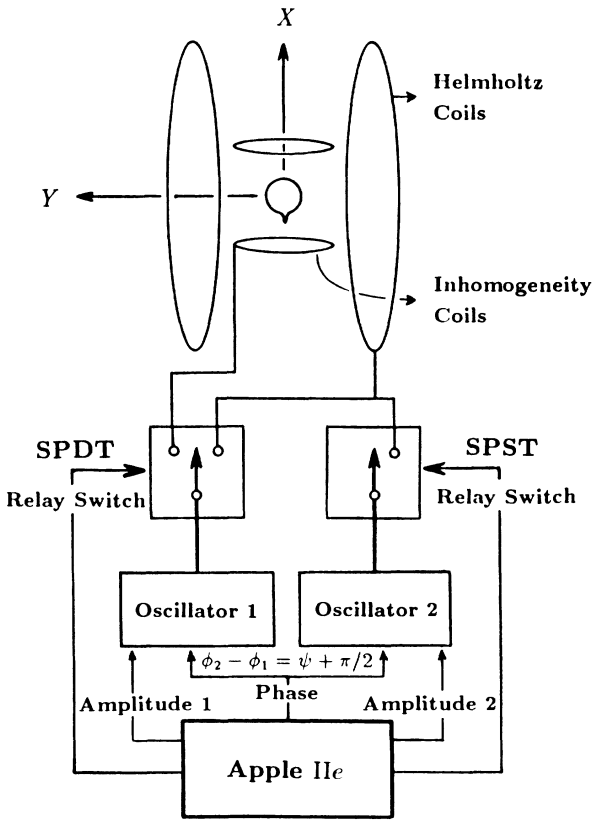

FIG. 9. Schematic diagram of the apparatus used to generate the data of Fig. 8. The oscillators 1 and 2 were used to produce homogeneous and inhomogeneous fields, in a sequence which was under the control of an Apple IIe computer. Details of the pulse sequences are discussed in the text in connection with Fig. 10.

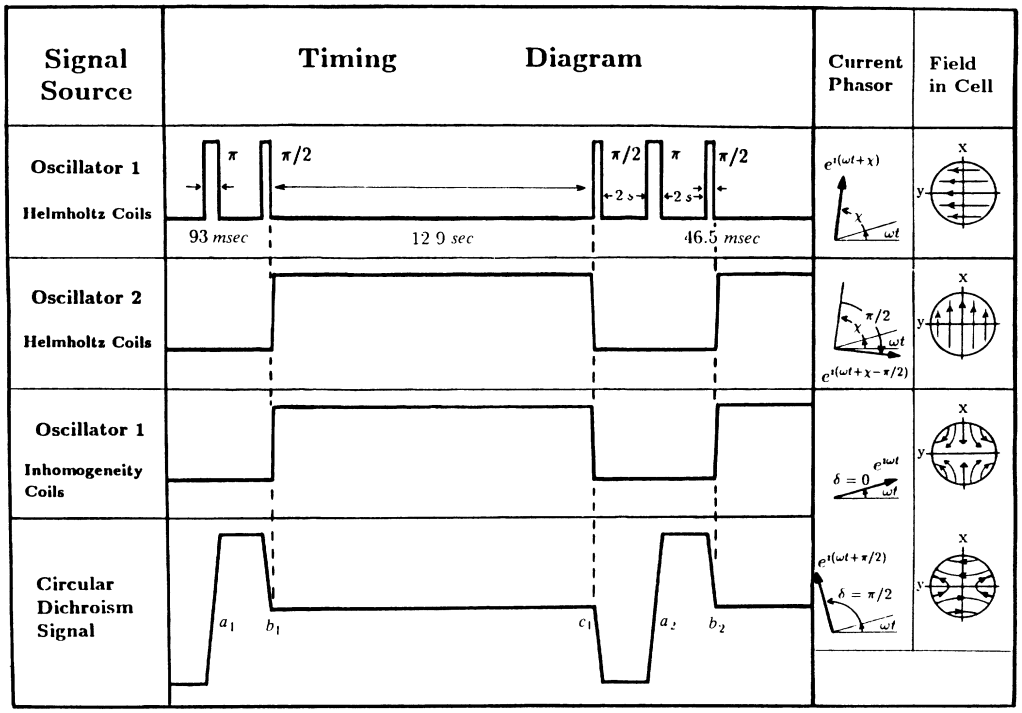

FIG. 10. Pulse sequences used to measure $1/T_{r1}$, the longitudinal relaxation rate in the rotating coordinate system. Oscillator 1 was used to produce π and $\pi/2$ pulses, by driving the Helmholtz coils of Fig. 9. Oscillator 1 was also used with an optional phase retardation ψ to drive inhomogeneity coils to cause spin relaxation. Oscillator 2 was used only provide a quantizing magnetic field along the x axis of the rotating coordinate system. Currents induced in the aluminum supports of the Helmholtz coils caused the field at the cell to lag the current in the drive coils by angle $\chi \approx 45°$. During the intervals from b_n to c_n a current from oscillator 1 passed through the inhomogeneity coils, and the resulting inhomogeneous field caused the spins to relax at a rate which depended on the phase $\delta = \chi - \psi$ of the current. As we have indicated in the sketch, the effective field seen by the spins was curl-free for $\delta = 0$, and it was divergence-free for $\delta = \pi/2$.

affect the measured relaxation rates.

Denote the current produced by oscillator 1 in the Helmholtz coils by

$$I(t) = I_1 \cos(\omega t + \chi) , \tag{82}$$

where the real, positive current amplitude is I_1. The field produced by the current (82) is

$$\mathbf{B} = \frac{2\Omega_a}{\lambda} \mathbf{y} \cos\omega t = \mathbf{B}_2' \cos\omega t , \tag{83}$$

where the gyromagnetic ratio λ was given by (73). Comparing (83) with (40) and noting that the field was exactly on resonance so $\omega = \Omega_0 = 129.3 \text{ Hz} \times 2\pi$, we see that

$$\boldsymbol{\Omega}_a = \Omega_a \mathbf{y} . \tag{84}$$

The spins could therefore be rotated about the **y** axis by the current (82). To produce $\pi/2$ rotations of the spins about the **y** axis we gated the current (82) on at the time of a zero crossing, and turned it off after six cycles of the oscillating field. The rotation frequency was $\Omega_a = 5.38 \text{ Hz} \times 2\pi = \Omega_0/24$. The gate-on time, 46.5 msec, was chosen to be a multiple of the internal clock interval of the computer. The current amplitude was empirically adjusted to make the rotation as close as possible to $\pi/2$ rad. To produce a spin rotation by π rad about the **y** axis, we gated the current on for 12 cycles or 93 msec.

At the beginning of the probe phase, we applied a π pulse, which occurred at the point labeled a_1 in Fig. 8, to invert the spins and to obtain a value for the initial polarization. After a delay of 2 sec to obtain a reading of the signal, we applied a $\pi/2$ pulse to orient the spins with the x axis. The time of application of the first $\pi/2$ pulse is indicated by b_1 in Fig. 8. Immediately after the $\pi/2$ pulse, a homogeneous quantizing field was applied along the x axis by gating the current

$$I(t) = I_2 \sin(\omega t + \chi) \tag{85}$$

from oscillator 2 into the Helmholtz coils. The amplitude of the current was such that it produced the field

$$\mathbf{B} = 2\omega_r \mathbf{y} \sin\omega t = \mathbf{B}_2'' \sin\omega t . \tag{86}$$

Comparing (86) and (40) we conclude that the quantizing field was

$$\boldsymbol{\Omega}_a = \omega_r \mathbf{x} . \tag{87}$$

The basis vectors of Fig. 1 can therefore be chosen to be

$$\mathbf{w} = \mathbf{x}, \quad \mathbf{u} = -\mathbf{z}, \quad \mathbf{v} = \mathbf{y} . \tag{88}$$

As a result of slight angle errors in the $\pi/2$ pulse, the spin polarization was not quite parallel to the x axis, and the

perpendicular part of the polarization rotated at the Rabi frequency ω_r about the x axis. The projection of this rotating component onto the z axis produced small oscillations of the circular dichroism signal, which can be seen between the points b_1 and c_1 of Fig. 8.

At the same time (the point b_1 of Fig. 8) that the quantizing field from oscillator 2 was applied to the Helmholtz coils, the phase angle of oscillator 1 was retarded by an angle ψ, so that the current from the oscillator was

$$I(t)=I_1\cos(\omega t+\delta)\ , \tag{89}$$

where the phase angle δ is

$$\delta=\chi-\psi\ . \tag{90}$$

The current from oscillator 1 passed through inhomogeneity coils, which had an axis of symmetry along the **x** direction, and which therefore produced a gradient described by (66). The coil supports were nonconducting plastic, and were much smaller than the supports for the Helmholtz coils, so the inhomogeneous field was very nearly in phase with the driving current and, according to (62), it could be written as

$$\mathbf{B}=\mathbf{r}\cdot\nabla\mathbf{B}=\kappa I_1\mathbf{r}\cdot(3\mathbf{xx}-1)(\cos\omega t\cos\delta-\sin\omega t\sin\delta)\ . \tag{91}$$

Comparing (91) with (41) we conclude that

$$\mathbf{\Omega}_c=\frac{\lambda\kappa I_1}{2}\mathbf{r}\cdot(3\mathbf{xx}-1)(\cdot[\mathbf{xx}+\mathbf{yy}]\cos\delta-\times\mathbf{z}\sin\delta)\ . \tag{92}$$

Multiplying out (92) and using (88) to evaluate the propagations of $\mathbf{\Omega}_c$ we find

$$\begin{aligned}\Omega_{cu}&=\Omega_{cz}=0\ ,\\ \Omega_{cv}&=\Omega_{cy}=\frac{\lambda\kappa I_1}{2}(2x\sin\delta-y\cos\delta)\ ,\\ \Omega_{cw}&=\Omega_{cx}=\frac{\lambda\kappa I_1}{2}(2x\cos\delta+y\sin\delta)\ .\end{aligned} \tag{93}$$

The effective field $\mathbf{B}_c=\lambda^{-1}\mathbf{\Omega}_c$ therefore lies in the uv plane (or the xy plane). The field depends on the phase angle δ, and we note that $\nabla\cdot\mathbf{B}_c=\frac{1}{2}\kappa I_1\cos\delta$ and $\nabla\times\mathbf{B}_c=(\mathbf{z}/2)\kappa I_1\sin\delta$. The gradient tensor is not traceless and symmetric, that is, divergence-free and curl-free because we neglected field components which are not static in the rotating coordinate system. For example, the divergence of the field is proportional to the number of rotating field lines which leave the xy plane and bend into the direction of the z axis. The field lines for $\delta=0$ and $\pi/2$ are sketched in Fig. 10.

Substituting (93) into (55) we find that the theoretically predicted value for the longitudinal relaxation rate during the 12.9-sec intervals from b_n to c_n of Fig. 8 is

$$\frac{1}{T_{r1}}=\frac{1}{\tau_1}\gamma_r=\frac{8}{175}r\,g(r,0)\gamma_r\ , \tag{94}$$

where the characteristic rate is

$$\gamma_r=\frac{(\lambda\kappa RI_1)^2}{4\omega_r}(1+3\sin^2\delta)\ . \tag{95}$$

and r is the relative Rabi frequency of (60).

At the points c_n in Fig. 8 the currents in the Helmholtz coils and in the inhomogeneity coils were turned off. The phase retardation ψ was eliminated and oscillator 1 was used to drive a second $\pi/2$ pulse through the Helmholtz coils and to rotate the spins into alignment with the negative z axis, where they produced an observable circular dichroism signal in the 2-sec interval between c_n and a_{n+1}.

Since no field inhomogeneity was applied during the intervals between the points c_n and b_{n+1}, most of the spin relaxation occurred in the intervals from the points b_n to c_n, during which time the spin polarization was along the quantization axis $\mathbf{w}=\mathbf{x}$ of the rotating coordinate system. We therefore assumed that the inversion signals, which occur at the points a_n, where attenuated by a factor $\exp[-(12.9\text{ sec})/T_{r1}]$ between successive inversions, and we analyzed data such as that of Fig. 8 accordingly to determine values of T_{r1}.

Keeping all other experimental parameters fixed, we measured $1/T_{r1}$ as a function of the phase angle δ, of (90). The results are shown in Fig. 10. There is excellent agreement with the $1+3\sin^2\delta$ dependence on δ predicted by (94) and (5), and the data can be used to infer that the phase retardation of the field with respect to the drive current of the Helmholtz coils was $49°\pm5°$, in agreement with direct measurements with pickup coils.

To facilitate comparison of our data with theory, we defined an experimental reduced rate $1/\tau_1$, analogous to (77), by

$$\frac{1}{\tau_1}=\frac{1}{\gamma_r T_{r1}}\ , \tag{96}$$

where the characteristic rate γ_r was defined by (95). From inspection we see that the theoretical reduced rate defined by (94) depends on r in exactly the same way as the theoretical reduced rate (79) depends on p/p^*. Consequently, we should find that the experimental reduced rate (96) will lie on the same curve, if plotted against r, as the experimental reduced rate (77), if plotted against p/p^*.

We measured $1/T_{r1}$ for absolute Rabi frequencies $\omega_r/2\pi$ ranging from 0.52 to 12.9 Hz. At each value of ω_r we measured $1/T_{r1}$ for five or six different drive currents I_1 in the inhomogeneity coils. The currents ranged from 1 to 20 mA. Experimental values of $1/\tau_1$ for different inhomogeneity currents at the same value of r were averaged and plotted in Fig. 7 as triangular data points. The predicted low-pressure relaxation rate data are proportional to R^4, and the cell was not quite spherical since it had a small internal stem at the point where it was sealed off from the filling manifold. We therefore let R be a free parameter and adjusted it to get a good fit between experiment and theory. The fitted value of $R=0.56$ cm which gave a good fit to the data was within experimental error the same as the value $R=0.55$ cm that we measured with calipers.

We have also used the oscillating, inhomogeneous magnetic field described above to measure the transverse relaxation rates $1/T_{r2}$ in the rotating frame. The experi-

mental procedure was very simple. After polarizing the ^{129}Xe nuclei by spin exchange optical pumping for an appropriate time, oscillator 2 provided a driving current of the form (85) for the Helmholtz coils and oscillator 1 provided a current of the form (82) for the inhomogeneity coils with $\delta=\chi=45°$. Transients similar to the one labeled $s=0$ in Fig. 4 were observed in the circular dichroism signal. The Rabi frequency could be determined directly from the frequency of the damped sinusoid. At high Rabi frequencies, it was not possible to record the signal directly with a chart recorder because the bandwidth limitations, and the signal envelope was recorded with a lock-in detector tuned to the Rabi frequency.

To facilitate comparison of our data with theory, we defined an experimental reduced relaxation rate $1/\tau_2$ in analogy to (96),

$$\frac{1}{\tau_2}=\frac{1}{\gamma_r T_{r2}} , \tag{97}$$

where the characteristic rate γ_r was defined by (95). As described above, measurements were made for several different drive currents I_1 in the inhomogeneity coils at each Rabi frequency. Experimental values of $1/\tau_2$ for different inhomogeneity currents at the same value of r were averaged and plotted in Fig. 7 as square data points. Substituting (93) into (55) we find for $\delta=45°$, $L=1$, and $M=1$ that the theoretical rate is

$$\frac{1}{\tau_2}=\frac{4r\,g(r,0)+8r}{175} . \tag{98}$$

The theoretical curve (98) is plotted in Fig. 7 for $p/p^*=r$.

IV. CONCLUSIONS

The experiments reported here show that it is possible to quantitatively understand how inhomogeneous magnetic fields cause spin relaxation in gases. Some of the important points which we have demonstrated are as follows.

(1) When spins are subject to an oscillating magnetic field which has a frequency close to the magnetic resonance frequency, the spin relaxation is characterized by a longitudinal relaxation rate $1/T_{r1}$ and a transverse relaxation rate $1/T_{r2}$ in the rotating frame. At exact magnetic resonance, theory predicts and our experiments confirm that for relaxation due to static field inhomogeneities, $1/T_{r1}=2/T_{r2}=1/T_2$, where $1/T_2$ is the transverse relaxation rate in the laboratory frame. As the oscillation frequency is detuned from exact resonance, the longitudinal relaxation rate $1/T_{r1}$ decreases rapidly toward $1/T_1$, the much smaller longitudinal relaxation rate in the laboratory frame. The transverse relaxation rate $1/T_{r2}$ approaches $1/T_2$ for large detunings (see Fig. 4). Figures 2 and 4 also show why the inversion of spins must be "fast" in an adiabatic fast passage experiment. If the passage through resonance is done too slowly to increase the adiabaticity of the process, the spin polarization can be significantly degraded by the greatly enhanced longitudinal relaxation rate at resonance.

(2) Under magnetic resonance conditions only three of the five independent components of a static magnetic field gradient have a large effect on spin relaxation. The three important parts of the gradient tensor are $\partial B_z/\partial x=\partial B_x/\partial z$, $\partial B_z/\partial y=\partial B_y/\partial z$, and $\partial B_z/\partial z$. The two unimportant parts of the gradient tensor are $\partial B_x/\partial y=\partial B_y/\partial x$ and $\partial B_x/\partial x=-\partial B_y/\partial y-\partial B_z/\partial z$. It is therefore possible to use currents in three independent pairs of inhomogeneity coils, for example, the coils described by (68), (70), (71) to cancel the major part of the relaxation due to inhomogeneous fields (see Fig. 5).

(3) An oscillating, inhomogeneous magnetic field with a frequency close to the magnetic resonance frequency of the spins can be very effective in causing spin relaxation in the rotating coordinate system. If the inhomogeneous oscillating field is coherent with the homogeneous oscillating field that establishes the quantization axis of the rotating frame, the relative phase of the two fields can have a large effect on the relaxation rate (see Fig. 11).

(4) Motional narrowing of $1/T_{r2}$ occurs as the relative Rabi frequency $r=\omega_r R^2/D$, or equivalently, the relative pressure p/p^*, decreases. There is also motional narrowing of $1/T_{r1}$ for $r\lesssim 1$, that is, when the characteristic diffusion rate D/R^2 across a spherical cell of radius R is faster than the absolute Rabi frequency ω_r (see Fig. 7).

(5) The predicted rates of spin relaxation due to magnetic field inhomogeneities depend on the diffusion constant D of the spins in the gas, on the physical dimensions of the sample cell, on the strength of the homogeneous and inhomogeneous magnetic fields, and on the frequency of any oscillating fields. These quantities are usually well known, except for the diffusion constant. Spin relaxation in inhomogeneous magnetic fields can therefore be used as a powerful new way to measure diffusion constants. We think that measurements of either $1/T_1$ or $1/T_{r2}$ at

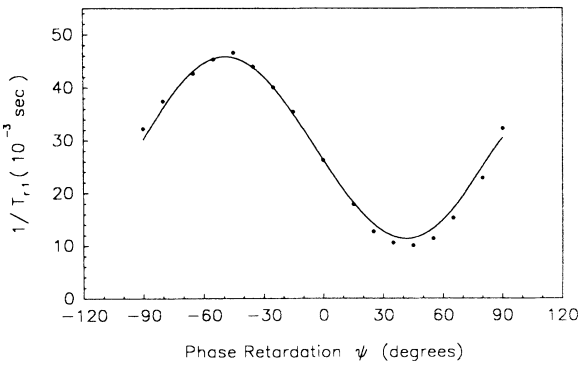

FIG. 11. Measured values of the longitudinal spin relaxation rate in the rotating coordinate system as a function of the phase retardation ψ of the drive current in the inhomogeneity coils (see Fig. 10). In accordance with the predictions of (94) and (95), the data were fit to a function of the form $1/T_{r1}=C[1+3\sin^2(\chi-\psi)]$ with C and χ as free parameters. The peak relaxation rate occurred when $\delta=\chi-\psi=\pi/2$ and the effective inhomogeneous field $\mathbf{B}_c=\boldsymbol{\Omega}_c/\lambda$ of (94) was divergence-free. The minimum relaxation rate occurred when $\delta=0$ and $\mathbf{B}_c$ was curl-free.

high effective pressure would be most convenient for determining diffusion constants because of the simplicity of the experimental procedure, and because the cell geometry has only a minor effect on the analysis.

(6) In this paper we used the lowest, nonvanishing order of perturbation theory to calculate the effects of magnetic field inhomogeneities on the spin relaxation. In the experiments described here, the field inhomogeneities (7) and (8) are small compared to the "energy denominators" of (21), provided that the energy denominators involve a change in the polarization quantum number M of (17). If M does not change, the denominator can be on the order of D/R^2 and, for small D, can be comparable to or smaller than the inhomogeneity matrix elements. Thus it may be necessary to incude the effects of higher-order terms in the perturbation calculation for high relative pressures.

ACKNOWLEDGMENT

This work was supported by the U.S. Air Force Office of Scientific Research under Grant No. 88-0165.

[1]G. D. Cates, S. R. Schaefer, and W. Happer, Phys. Rev. A **37**, 2877 (1988).
[2]R. L. Gamblin and T. R. Carver, Phys. Rev. **138**, 946 (1965).
[3]L. D. Schearer and G. K. Walters, Phys. Rev. **139**, 1398 (1965).
[4]R. Barbé, M. Leduc, and F. Laloë, Nuovo Cimento Lett. **8**, 915 (1973).
[5]R. Barbé, M. Leduc, and F. Laloë, J. Phys. (Paris) **35**, 699 (1974); **35**, 935 (1974).
[6]V. Lefèvre-Seguin, P. J. Nacher, and F. Laloë, J. Phys. (Paris) **43**, 737 (1982).
[7]U. Fano, Rev. Mod. Phys. **29**, 74 (1957).
[8]Z. Wu, S. R. Schaefer, G. D. Cates, and W. Happer, Phys. Rev. A **37**, 1161 (1988).
[9]M. E. Rose, *Elementary Theory of Angular Momentum* (Wiley, New York, 1957).
[10]F. Bloch and A. Siegert, Phys. Rev. **57**, 522 (1940).
[11]I. I. Rabi, N. F. Ramsey, and J. Schwinger, Rev. Mod. Phys. **26**, 167 (1954).
[12]E. B. Aleksandrov, O. V. Konstantinov, V. I. Perel', and V. A. Khodovoi, Zh. Eksp. Teor. Fiz. **45**, 503 (1963) [Sov. Phys.—JETP **18**, 346 (1964)].
[13]C. J. Favre and E. Geneux, Phys. Lett. **8**, 190 (1964).
[14]C. Cohen-Tannoudji, J. Dupont-Roc, S. Haroche, and F. Laloë, Phys. Rev. Lett. **22**, 758 (1969).
[15]B. C. Grover, Phys. Rev. Lett. **40**, 391 (1978).
[16]C. H. Volk, T. M. Kwon, and J. G. Mark, Phys. Rev. A **21**, 1549 (1980).
[17]W. Happer, E. Miron, S. R. Schaefer, D. Schreiber, W. A. van Wijngaarden, and X. Zeng, Phys. Rev. A **29**, 3092 (1984).
[18]X. Zeng, Z. Wu, T. Call, E. Miron, D. Schreiber, and W. Happer, Phys. Rev. A **31**, 260 (1985).
[19]Z. Wu, W. Happer, and J. Daniels, Phys. Rev. Lett. **59**, 480 (1987).
[20]The work discussed in this section was carried out by one of us (D.J.W.) as part of a Senior thesis, Princeton University, 1988.